chemosensors

MDPI

Article

Nanocrystalline Oxides $Ni_xCo_{3-x}O_4$: Sub-ppm H_2S Sensing and Humidity Effect

Kseniya Prikhodko [1], Abulkosim Nasriddinov [1,2], Svetlana Vladimirova [1], Marina Rumyantseva [1,*] and Alexander Gaskov [1]

[1] Chemistry Department, Moscow State University, 119991 Moscow, Russia; k.prikhodko@live.ru (K.P.); naf_1994@mail.ru (A.N.); vladimirova.lagytina@gmail.com (S.V.); gaskov@inorg.chem.msu.ru (A.G.)
[2] Faculty of Materials Science, Moscow State University, 119991 Moscow, Russia
* Correspondence: roum@inorg.chem.msu.ru; Tel.: +7-495-939-5471

Abstract: In this work, *p*-type oxide semiconductors, Co_3O_4 and complex oxides $Ni_xCo_{3-x}O_4$ (x = 0.04, 0.07, 0.1), were studied as materials for sub-ppm H_2S sensing in the temperature range of 90–300 °C in dry and humid air. Nanocrystalline Co_3O_4 and $Ni_xCo_{3-x}O_4$ (x = 0.04, 0.07, 0.1) were prepared by coprecipitation of cobalt and nickel oxalates from nitrate solutions and further annealing at 300 °C. The surface reactivity of the obtained materials toward H_2S both in dry and humid atmosphere (relative humidity at 25 °C R.H. = 60%) was investigated using diffuse reflectance infrared Fourier transform spectroscopy (DRIFTS). Sensor measurements showed a decrease in sensor signal toward 1 ppm H_2S with an increase in Ni content because of a decrease in chemisorbed surface oxygen species. On the other hand, sensor signal increases for all samples with increasing the relative humidity that depends on reactivity of the surface hydroxyl groups, which stimulate the decomposition of surface sulfites and provide better surface regeneration at higher temperature. This assumption was additionally confirmed by the faster saturation of the conductivity curve and a decrease in the sensor response time in humid air.

Keywords: cobalt oxide Co_3O_4; complex oxides $Ni_xCo_{3-x}O_4$; hydrogen sulfide H_2S; semiconductor gas sensor; humidity effect; DRIFTS investigation

Citation: Prikhodko, K.; Nasriddinov, A.; Vladimirova, S.; Rumyantseva, M.; Gaskov, A. Nanocrystalline Oxides $Ni_xCo_{3-x}O_4$: Sub-ppm H_2S Sensing and Humidity Effect. *Chemosensors* **2021**, *9*, 34. https://doi.org/10.3390/chemosensors9020034

Academic Editor: Jose Vicente Ros Lis
Received: 31 December 2020
Accepted: 2 February 2021
Published: 7 February 2021

1. Introduction

Hydrogen sulfide is a highly toxic, reactive and flammable gas that is found in various technological processes. Therefore, it is extremely important to monitor its concentration in the air at a level below 100 ppm of H_2S, which is considered to be immediately dangerous to life and health (IDLH). Semiconductor gas sensors based on *n*-type metal oxides are one of the most commonly used commercial hydrogen sulfide detectors [1]. For this type of devices, the problem of the negative influence of ambient humidity often arises [2,3]. The effect of humidity had been actively studied for the most common oxides used in gas sensors, such as SnO_2 [4,5], WO_3 [6], ZnO [7], In_2O_3 [8]. The blocking effect of adsorbed water on WO_3 can be overcome by aging processes, leading to the appearance of surface hydroxyl groups [9].

Currently, there are different types of gas sensors with great potential for use in "e-nose" systems and "smart sensors" [10–12]. However, the attention of researchers is increasingly attracted by less common sensors based on p-type oxides, such as CuO, NiO, Co_3O_4. In particular, an increase in the sensor signal in the presence of moisture was observed for CuO sensors used for H_2S detection in a hydrogen atmosphere [13]. This effect was associated with the formation of hydroxyl groups due to the water dissociation on the oxide surface.

Dissociation of water molecules and the formation of strongly bonded hydroxyl groups coordinated at metal centers were also observed on well-ordered Co_3O_4 (111) film [14]. Similar processes can be expected on the surface of polycrystalline Co_3O_4 (Figure 1). In this

case, hydroxyl groups can act as oxidizing agents, which can lead to additional oxidation processes in humid air.

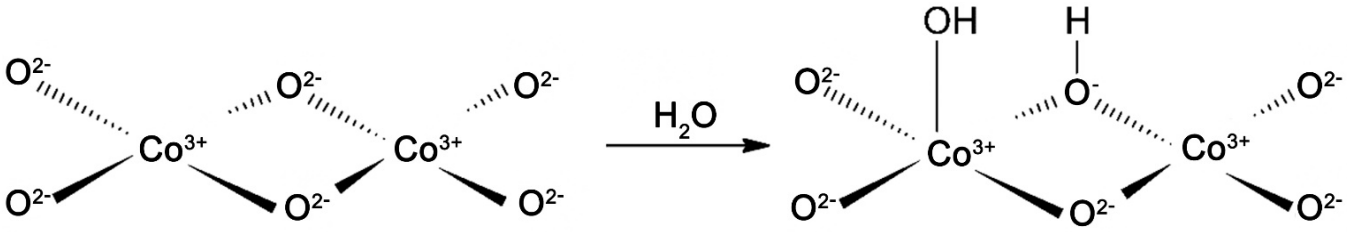

Figure 1. The dissociation of water molecule on Co_3O_4 surface.

Cobalt oxide Co_3O_4 with a spinel structure has a high catalytic activity in oxidation reactions, which is provided by the high concentration of chemisorbed oxygen on the oxide surface. O_2 molecules are adsorbed on the surface oxygen vacancy sites, forming reactive oxygen species (ROS), such as O_2^- and O_2^{2-} (Figure 2). It is assumed that these ROS are involved in the catalytic oxidation of hydrocarbons [15], CO [16,17] and formaldehyde [18] above Co_3O_4.

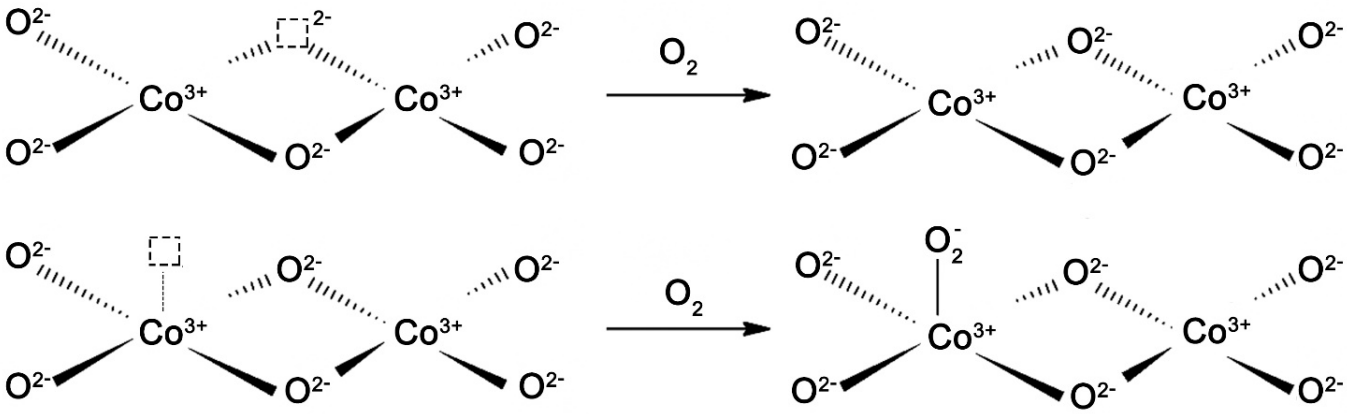

Figure 2. Formation of ROS on the Co_3O_4 surface.

One of the main limitations of Co_3O_4 as a material for gas sensors is its high electrical resistance. The introduction of nickel into the spinel structure with the formation $Ni_xCo_{3-x}O_4$ ($x \leq 1$) leads to a sharp drop in resistance of the material, which is realized due to an increase in the mobility of charge carriers at $x \leq 0.25$ [19]. At the same time, a decrease in the concentration of chemisorbed oxygen is observed, correlating with a decrease in the proportion of Co^{3+} in octahedral positions. This leads to a drop in the CO sensor signal with an increase in the proportion of nickel.

The aim of the present study is to investigate the sensor properties of cobalt oxide Co_3O_4 and complex oxides $Ni_xCo_{3-x}O_4$ ($x \leq 0.1$) to hydrogen sulfide in humid air. Special attention is paid to the mechanism of reactions and the role of surface hydroxyl groups in these processes.

2. Materials and Methods

Nanocrystalline powders of Co_3O_4 and $Ni_xCo_{3-x}O_4$ (x = 0.04, 0.07, 0.1) were prepared by coprecipitation of cobalt and nickel oxalates from nitrate solutions, and their further annealing at 300 °C. Elemental analysis of the samples was performed by XRF and ICP-MS methods. In order to avoid standard errors of the results, obtained by XRF analysis, the calibration was performed using ICP-MS method on the quadrupole mass spectrometer Agilent 7500C. Isotopes ^{59}Co, ^{60}Ni and ^{58}Ni were used for determination of Co and Ni. A detailed description of this technique can be found in Ref. [20]. The phase composition, microstructure parameters and the charge state of cations were studied by XRD, TEM,

XPS, EPR, as well as BET measurements [19]. The main characteristics of the samples are presented in Table 1.

Table 1. Composition and microstructure parameters of Co_3O_4 and $Ni_xCo_{3-x}O_4$ samples.

Sample	$\frac{[Ni]}{[Ni]+[Co]}$, wt %	Structural Type/Lattice Constant *a* (Å)	XRD Particles Size d (nm)	BET Specific Surface Area S_{BET} (m^2 g^{-1})
Co_3O_4	0	normal spinel 8.0575(14)	11 ± 2	48 ± 3
$Ni_{0.04}Co_{2.96}O_4$	1.24 ± 0.06	normal spinel 8.0681(12)	12 ± 1	44 ± 3
$Ni_{0.07}Co_{2.93}O_4$	2.4 ± 0.1	normal spinel 8.0734(17)	9 ± 1	56 ± 4
$Ni_{0.1}Co_{2.9}O_4$	3.3 ± 0.2	normal spinel 8.0800(30)	10 ± 1	53 ± 3

The morphology of cobalt oxide was investigated by transmission electron microscopy (TEM) using a FEI Tecnai G2 30 UT microscope operated at 300 kV.

The gas sensor properties were determined by comparing the electrical resistance of thick films in dry or humid air (0, 20%, 60% R.H.) with the resistance in the presence of H_2S (0.07–1.3 ppm). The films were obtained by the following procedure: the synthesized powders were ground with a binder (a solution of α–terpineol in ethanol), and then the pastes were deposited on functional substrates with Pt contacts on the front side and a Pt-meander on the back side that acts both as a heating element and a temperature probe. After covering each layer, DC voltage of 5 V was applied for 2 min. Sensors were annealed at 300 °C for 24 h. The films obtained by this technique are uniform and continuous throughout the substrate, and their thickness is about 1 μm [21].

An automatic device that allowed controlling the temperature and the gas flows (100 mL/min in all experiments) was used for the measurements. Sensor properties were investigated in the temperature range 90–300 °C. For each temperature stage, at first pure air and then a mixture of the test gas and air was supplied into the chamber for 15 min. The cycle was repeated three times for each temperature stage. Pure air generator (Granat-Engineering Co. Ltd., Moscow, Russia) was used to produce purified carrier gas. In sensor measurements and DRIFTS investigations a relative humidity was set and measured by Humidifier P-2 (Cellkraft AB, Sweden). The sensor signal S was determined according to:

$$S = (R_g - R_a)/R_a, \quad (1)$$

From the averaged values of the resistance in air R_a and in the presence of the test gas R_g.

A Perkin–Elmer Frontier spectrometer provided with a DiffusIR annex and flow-through reactor with a furnace (HC900, Pike Technologies) sealed with the ZnSe window was used for in situ diffuse-reflectance infrared Fourier-transform (DRIFT) spectroscopy study of material interactions with H_2S. The spectra were recorded in the range of 4000–1000 cm^{-1} with a resolution of 1 cm^{-1} and averaging of 30 scans under control of the gas phase composition. The powders (50 mg) were placed in alundum crucibles 5 mm in diameter. The samples were heated in a flow of clean air at 300 °C before collecting the spectra. The sequence of recording conditions for Co_3O_4 is shown in Figure 3. A similar experiment was carried out for $Ni_{0.1}Co_{2.9}O_4$ sample. Hydrogen sulfide treatment was carried out at a temperature of 220 °C in a flow of H_2S (20 ppm, 100 mL/min) in dry air and in a humidity of 60% R.H. After 50 min of measurements, the temperature was raised to 300 °C and a flow of pure air was started.

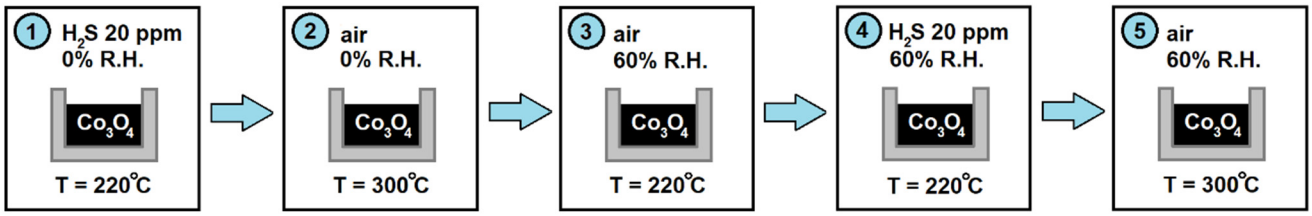

Figure 3. Diffuse-reflectance infrared Fourier-transform spectroscopy (DRIFTS) experimental scheme for Co_3O_4.

3. Results and Discussion

3.1. Characteristics of Nanocrystalline Co_3O_4 and $Ni_xCo_{3-x}O_4$ Samples

The microstructure of Co_3O_4 was investigated by TEM (Figure 4). The sample consists of aggregated particles (20–100 nm) and has a porous structure due to the release of gases (CO, CO_2) during the decomposition of the oxalate precursor.

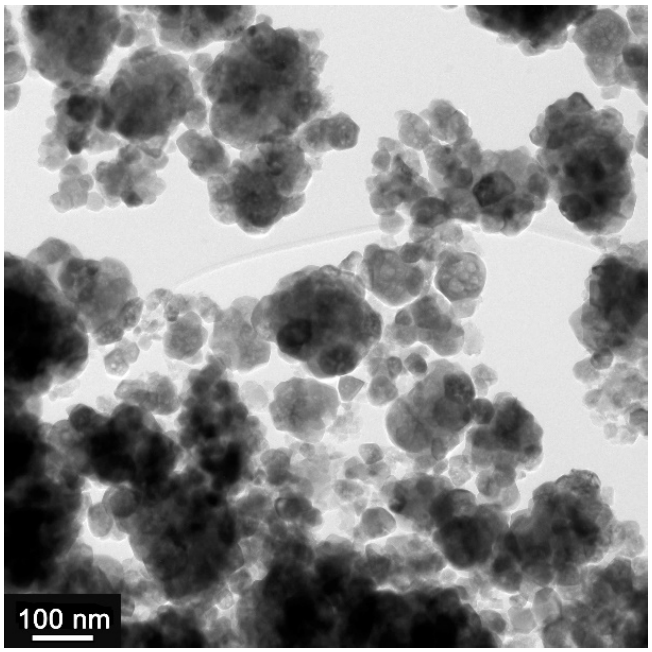

Figure 4. TEM image of Co_3O_4.

3.2. Sensor Properties for H_2S Detection

Initially the Co_3O_4 and $Ni_xCo_{3-x}O_4$ (x = 0.04, 0.07, 0.1) sensors were exposed to H_2S in dry air. In order to find the optimum conditions, the operating temperature was varied from 300 to 90 °C. Figure 5a shows a dynamic response of Co_3O_4 and $Ni_xCo_{3-x}O_4$ based gas sensors to the periodical change of gas phase composition from 1 ppm H_2S to dry air at 210 °C. There are 3 periodical changes in gas phase composition for every operating temperature, the flow of H_2S and dry air was supplied to the test chamber for strictly 15 min. All samples showed a typical response of *p*-type oxides towards a reducing gas such as hydrogen sulfide: the resistance growth in the presence of H_2S and returns back in dry air. The same type of response to H_2S was observed in the humid conditions at 300–90 °C (Figure 5b). All samples showed stable and well reproducible resistance changes and, accordingly, sensor signal.

The temperature dependencies of the sensor signal S (Figure 6a) with a maximum value in the region of 210–240 °C are very similar for all the samples. Therefore, this temperature range is the most favorable for H_2S detection. A maximum value of S = 1.1 was observed for Co_3O_4 at 210 °C.

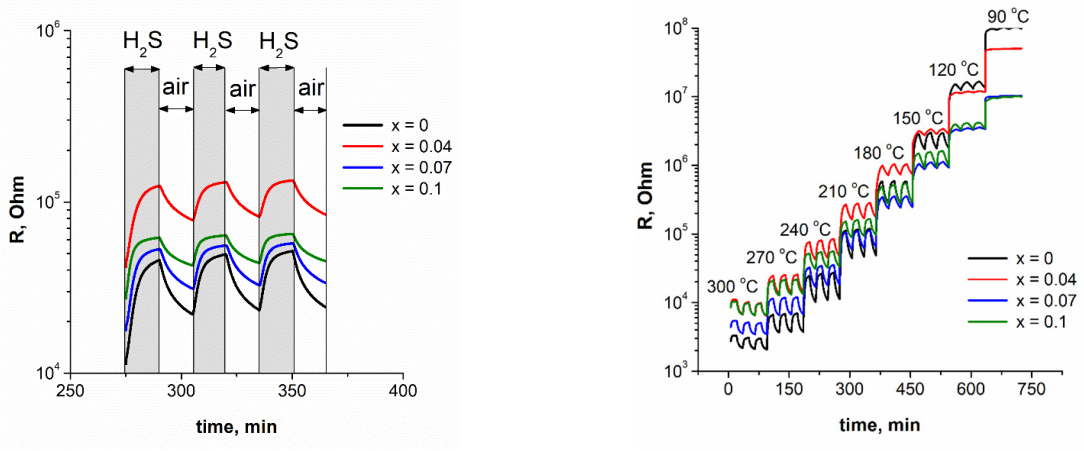

(**a**) (**b**)

Figure 5. Dynamic response of Co_3O_4 and $Ni_xCo_{3-x}O_4$ based gas sensors in the periodic presence of H_2S (1 ppm): (**a**) in dry air at 210 °C; (**b**) in humid air (60% R.H.) at 90–300 °C.

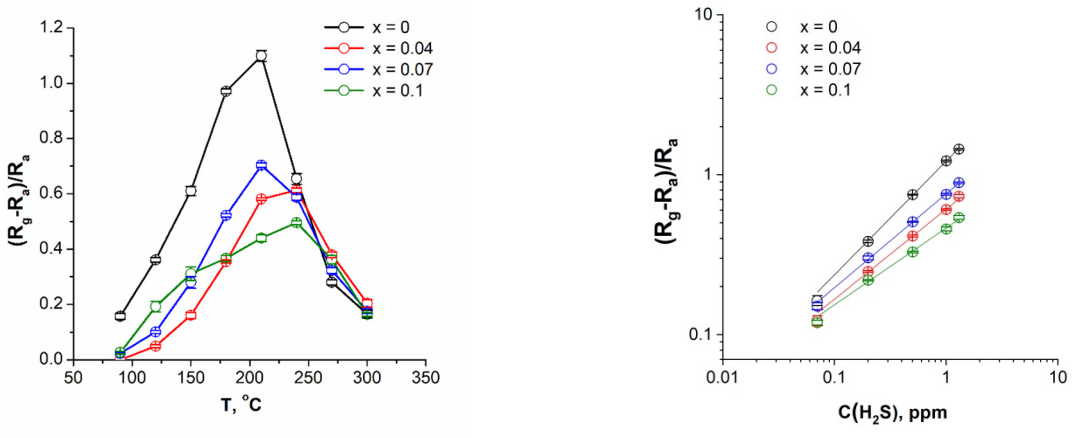

(**a**) (**b**)

Figure 6. (**a**) The temperature dependence of the sensor signal at the range of 90–300 °C in the presence of H_2S (1 ppm) in dry air; (**b**) Dependence of the sensor signal value on the concentration of H_2S at 210 °C in dry air.

The effect of hydrogen sulfide concentration was also studied at this temperature (210 °C). The lowest-observed-adverse-effect level of H_2S is 10 ppm, when the irritation of eyes, nose, and throat is caused. In order to prevent serious eye damage, a relatively high protection factor of 100 is used, which leads to a target value of 0.1 ppm with an averaging time of 24 h [22]. On the other hand, the human olfactory organ is able to sense the presence of hydrogen sulfide at a rather low concentration limit of about 0.008–0.13 ppm. Therefore, in this work, the range of target concentrations for Co_3O_4 and $Ni_xCo_{3-x}O_4$ samples were selected between 0.07 and 1.3 ppm, which indicates a high potential for use as an "electronic nose" system.

The dependences of the sensor signal S on the H_2S concentration were linearized in double logarithmic coordinates corresponding to the power law $S \sim C(H_2S)^n$ (Figure 6b). From these calibration curves the values of the lowest detectable concentration (LDC) for H_2S were determined (Table 2). The value $\frac{3\sigma}{R_{av}}$, where R_{av} is the average resistance value and σ is the standard deviation of the resistance in the air, was used as the minimum measurable response. A decrease in the sensitivity of $Ni_xCo_{3-x}O_4$ samples with increasing

Ni content is accompanied by a decrease in LDC from 120 to 100 ppb if a minimum amount of nickel is introduced.

Table 2. Lowest detectable concentration (LDC) of H_2S for sensors based on Co_3O_4 and $Ni_xCo_{3-x}O_4$ materials measured at 210 °C.

Sample	LDC, ppb	Sensitivity (Signal per Concentration), ppm^{-1}
Co_3O_4	120	0.74
$Ni_{0.04}Co_{2.96}O_4$	100	0.60
$Ni_{0.07}Co_{2.93}O_4$	150	0.60
$Ni_{0.1}Co_{2.9}O_4$	120	0.51

Further tests were carried out in humid air. As the R.H. value increases, the overall temperature dependence of the sensor signal is retained, but its value has increased. This effect was especially noticeable at temperatures above 210 °C (Figure 7a). The rise in the signal value was sharper for Co_3O_4 than for $Ni_xCo_{3-x}O_4$ samples (Figure 7b).

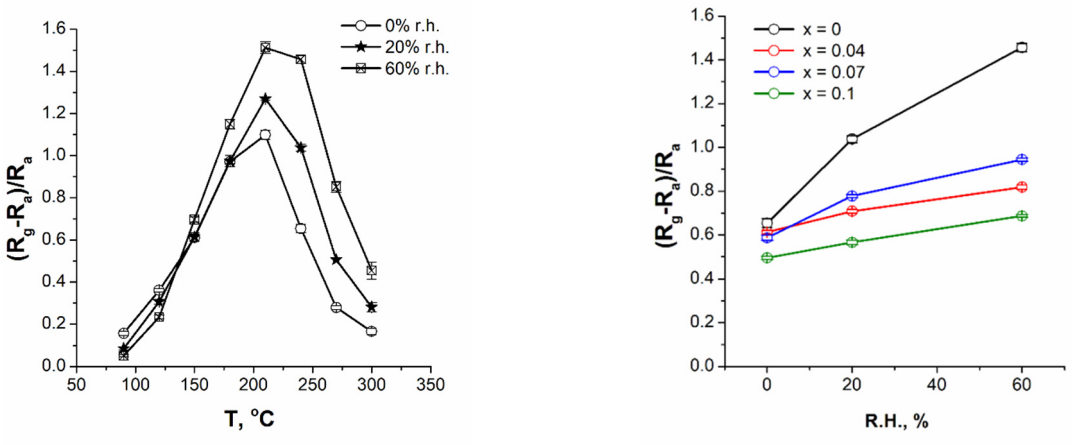

(**a**) (**b**)

Figure 7. (**a**) The temperature dependence of the sensor signal of Co_3O_4 at the range of 90–300 °C in the presence of H_2S (1 ppm) at different air humidity (0, 20, 60% R.H.); (**b**) Dependence of the sensor signal of Co_3O_4 and $Ni_xCo_{3-x}O_4$ on air humidity at 240 °C toward 1 ppm H_2S.

Figure 8a,b shows a comparison of the sensor signal value divided by gas concentration for H_2S, NH_3, and CO at 210 °C in dry air (0% R.H.) and humid atmosphere (30% R.H.), respectively. All samples show high sensitivity to H_2S, despite the fact that its concentration is 20 times less than the concentration of other gases. Further, it can be noticed that the sensitivity of H_2S increases in humid air, unlike ammonia and carbon monoxide. Most likely, the decisive contribution to the formation of an electric signal towards NH_3 and CO in dry and humid air is made only by the process of their oxidation with the participation of various chemisorbed oxygen species on the surface of complex oxides. During interaction with hydrogen sulfide in humid air, surface-adsorbed hydroxyl groups also make an additional contribution to the oxidation of H_2S molecules.

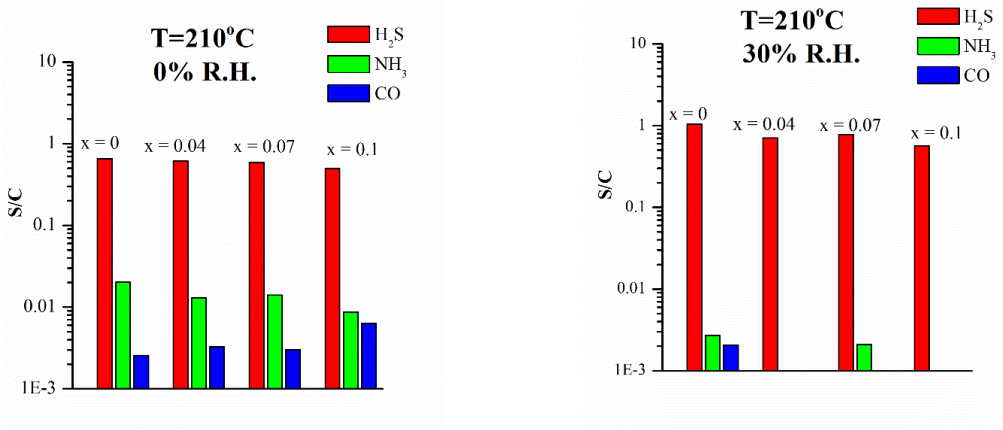

(**a**) (**b**)

Figure 8. The sensor signal toward 1 ppm H_2S, 20 ppm NH_3, 20 ppm CO (divided by gas concentration) of Co_3O_4 and $Ni_xCo_{3-x}O_4$ at 210 °C (**a**) 0% R.H. (**b**) 30% R.H.

3.3. DRIFT Spectroscopy Investigation in a Hydrogen Sulfide Atmosphere

3.3.1. Interaction of Co_3O_4 with H_2S in Dry Air

During adsorption of the hydrogen sulfide on the Co_3O_4 surface in dry air at the temperature of the maximum sensor signal, there was no absorption bands in the region of 2560–2580 cm^{-1} related to characteristic ν(SH) bands of adsorbed hydrogen sulfide molecules on the DRIFT spectra (Figure 9a) [23]. This fact indicates rapid oxidation of H_2S on the cobalt oxide surface, which can occur with the participation of chemisorbed oxygen or hydroxyl groups:

$$2H_2S_{(g)} + 3O_2{}^{2-} \rightarrow 2SO_{2(g)} + 2H_2O + 6e^-, \quad (2)$$

$$H_2S_{(g)} + 6OH^- \rightarrow SO_{2(g)} + 4H_2O + 6e^-. \quad (3)$$

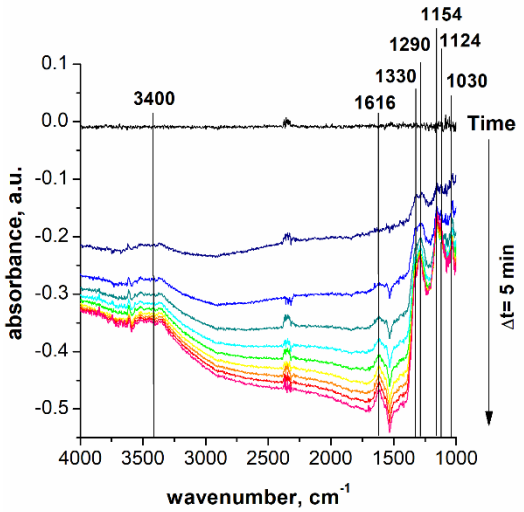

(**a**)

Figure 9. *Cont.*

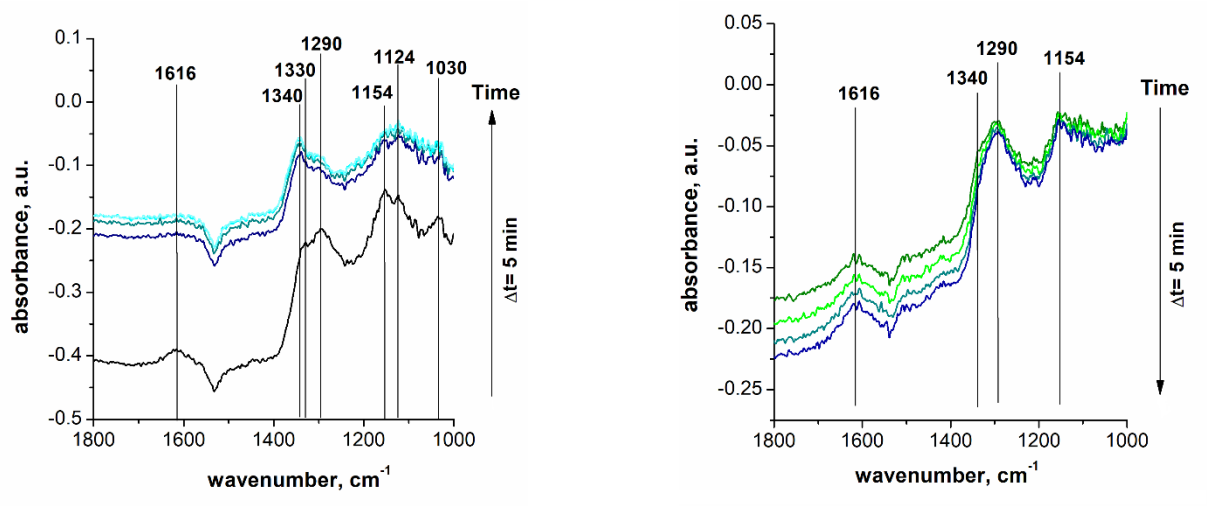

Figure 9. Co_3O_4 DRIFT spectra: (**a**) 20 ppm H_2S in dry air at 220 °C; (**b**) Annealing in dry air at 300 °C; (**c**) Humid air (60% R.H.) at 220 °C.

The products of H_2S oxidation appeared in the form of a complex absorption band at 1380–1000 cm^{-1}, which can correspond to S–O vibrations in sulfates, sulfites or adsorbed SO_2 [24–28]. Oxidation products, as well as adsorbed water molecules (1616 cm^{-1}) and hydroxyl groups (broad band at 3400 cm^{-1}) accumulated on the oxide surface during the experiment. The decreasing signal at 1530 cm^{-1} corresponds to surface nitrates (from the precursor [26]) consumed in the oxidation of hydrogen sulfide.

A more detailed analysis of changes in spectra over time, as well as varying temperature and humidity, allowed the determination of the composition of the oxidation products. Firstly, the bands at 1330, 1290, 1154 cm^{-1} and the vibrational mode of hydroxyl groups were observed. Then, there was a sharp increase in the intensity of the bands at 1290 and 1154 cm^{-1} and the appearance of the water signal and bands at 1124 and 1030 cm^{-1}. With an increase in temperature to 300 °C in a flow of dry air (Figure 9b), a new signal appeared at 1340 cm^{-1}, and the intensity of the remaining bands decreased. However, complete desorption of the products was not observed. In the presence of moisture (Figure 9c), the band at 1340 cm^{-1} disappeared, but the intensities of signals at 1290, 1154 cm^{-1} increased.

The low-frequency signal at 1030 cm^{-1} can be attributed to sulfite groups, which are formed through the SO_2 adsorption on the basic O_2^- centers (Figure 10a) on the oxides surface [23,28]. Under humid conditions, the adsorption of SO_2 also occurs on hydroxyl groups, resulting in the formation of HSO_3^- groups (Figure 10b). Thus, the bands at 1290 and 1154 cm^{-1} should be attributed to hydrosulfite groups, which correlates with the frequencies reported for HSO_3^- on zeolites [23,29]. The absorption at 1330 cm^{-1}, which is close to the asymmetric vibrations (ν_{as}) O=S=O, is probably associated with weakly chemisorbed SO_2 [27].

Temperature resistant bands at 1340 and 1124 cm^{-1} probably correspond to surface sulfate species [24,25], which were formed upon further oxidation of SO_2 or sulfites:

$$SO_3^{2-} + O_2^{2-} \rightarrow SO_4^{2-} + H_2O + 2e^-. \quad (4)$$

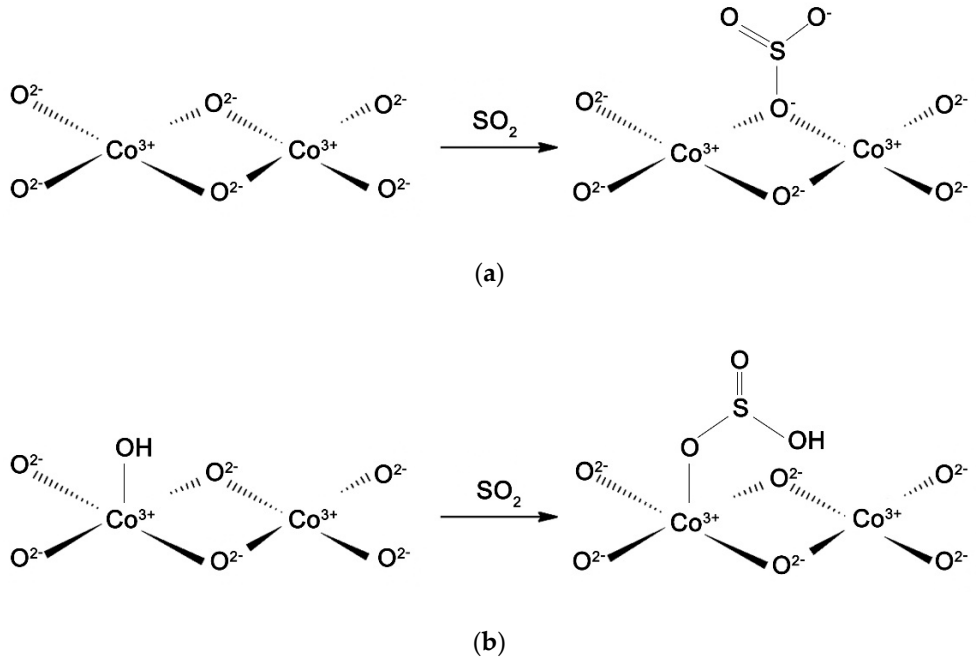

(**a**)

(**b**)

Figure 10. SO_2 adsorption on the Co_3O_4 surface: (**a**) on O_2^- centers; (**b**) on hydroxyl groups.

3.3.2. Interaction of Co_3O_4 with H_2S in Humid Air

DRIFT spectra of Co_3O_4 in a flow of H_2S in humid air (Figure 11a) are characterized by intense absorption bands of water (1621 cm^{-1}) and broad bands of hydroxyl groups (3430 cm^{-1}).

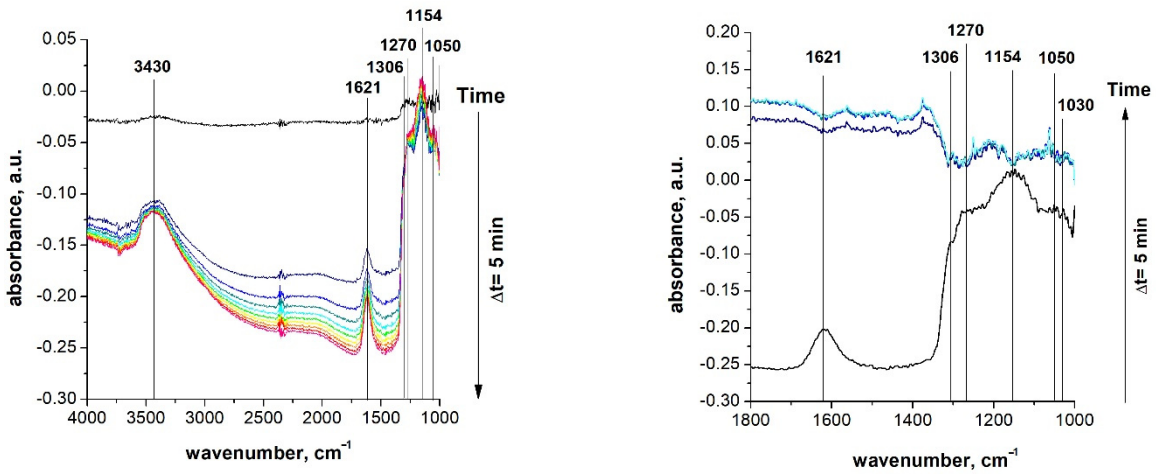

(**a**) (**b**)

Figure 11. Co_3O_4 DRIFT spectra: (**a**) 20 ppm H_2S in humid air (60% R.H.) at 220 °C; (**b**) Annealing in humid air (60% R.H.) at 300 °C.

In the flow of hydrogen sulfide, there was a rapid accumulation of hydrosulfite groups (1270 and 1154 cm^{-1}), as well as sulfites (1050 and 1030 cm^{-1}). The shoulder at 1306 cm^{-1} corresponds to weakly bounded SO_2 molecules [27].

Upon further annealing at 300 °C in humid air (Figure 11b), a rapid disappearance of the oxidation products signals was observed. The negative absorption bands (1306, 1270, and 1154 cm^{-1}) indicate decomposition of the sulfite groups remained on the cobalt oxide surface after supplying H_2S in dry air. Thus, the catalytic effect of water on the decomposition of surface sulfite groups takes place (Figure 12).

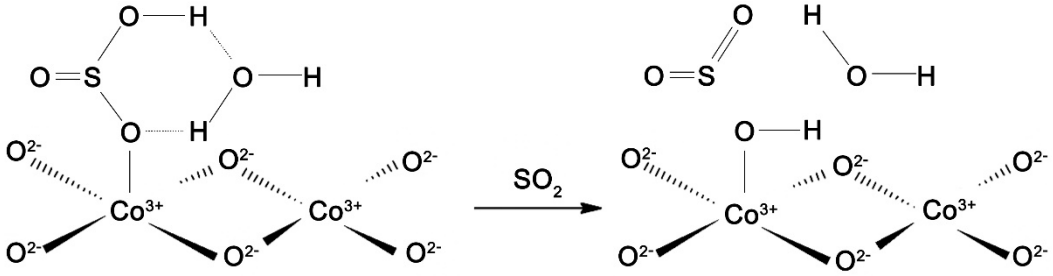

Figure 12. Decomposition of sulfites on Co_3O_4 in the presence of water.

3.3.3. Interaction of $Ni_{0.1}Co_{2.9}O_4$ with H_2S in Dry and Humid Air

In order to investigate the influence of Ni addition on the reactivity of Co_3O_4 with H_2S, the $Ni_{0.1}Co_{2.9}O_4$ sample has been chosen for DRIFT investigation. This sample has the maximum nickel content, which can significantly affect the surface active centers. DRIFT spectra of $Ni_{0.1}Co_{2.9}O_4$ (Figure 13) obtained at the same conditions are similar to those for Co_3O_4.

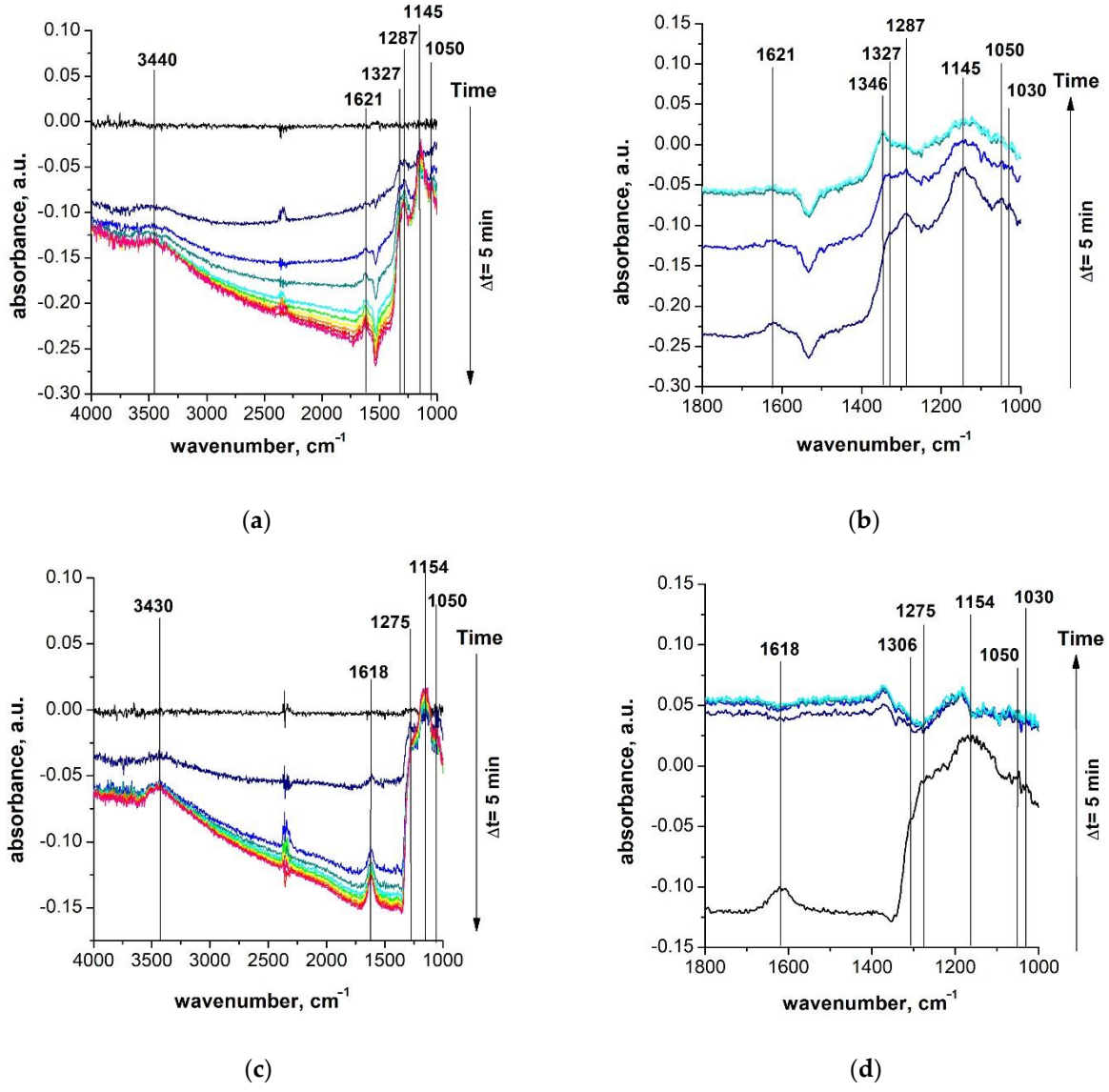

Figure 13. $Ni_{0.1}Co_{2.9}O_4$ DRIFT spectra: (**a**) 20 ppm H_2S in dry air at 220 °C; (**b**) Annealing in dry air at 300 °C; (**c**) 20 ppm H_2S in humid air (60% R.H.) at 220 °C; (**d**) Annealing in humid air (60% R.H.) at 300 °C.

Comparing the absorption modes of $Ni_{0.1}Co_{2.9}O_4$ with Co_3O_4 spectra (Table 3), a shift to the low-frequency region of a number of bands was noticed. In general, the introduction of nickel into the structure did not distinctly affect the H_2S oxidation process and the adsorption of products on the sample surface.

Table 3. Absorption bands on Co_3O_4 and $Ni_{0.1}Co_{2.9}O_4$ DRIFT spectra.

Surface Groups	Adsorption Bands, cm^{-1}			
	Co_3O_4		$Ni_{0.1}Co_{2.9}O_4$	
	0% R.H.	60% R.H.	0% R.H.	60% R.H.
OH	3400 (broad.)	3430 (broad.)	3440 (broad.)	3430 (broad.)
H_2O	1616	1621	1621	1618
SO_4^{2-}	1340, 1124	–	1346	–
SO_3^{2-}	1030	1030, 1050	1030, 1050	1030, 1050
HSO_3^-	1290, 1154	1270, 1154	1287, 1145	1275, 1154
$SO_{2(ads)}$	1330	1306	1327	1306

3.3.4. DRIFT Spectra Baseline Absorption and Sensor Signal

For semiconductor compounds, part of the infrared absorption occurs on free carriers. From the Drude-Zener theory it can be shown [30,31] that the absorption at a given wavelength A(λ) is directly related to the electrical conductivity of the material:

$$A(\lambda) = \sigma(\lambda)z/\varepsilon_0\, c\, n, \quad (5)$$

where σ (λ) is the electrical conductivity depending on the wavelength, z is the thickness of the sample, ε_0 is the permittivity of the vacuum, c is the velocity of light, and n is the refractive index of the material.

Since the DRIFT spectra were recorded on the same sample, the change in the baseline intensity is associated with a change in the electrical conductivity of the sample, and hence its resistance. This allows us to relate the change in the absorption intensity of the baseline (Figure 14) and the resistance of the samples in the sensor experiments. Moreover, the change in resistance in both cases was caused by the processes of oxidation of hydrogen sulfide and adsorption of products on the surface of oxides.

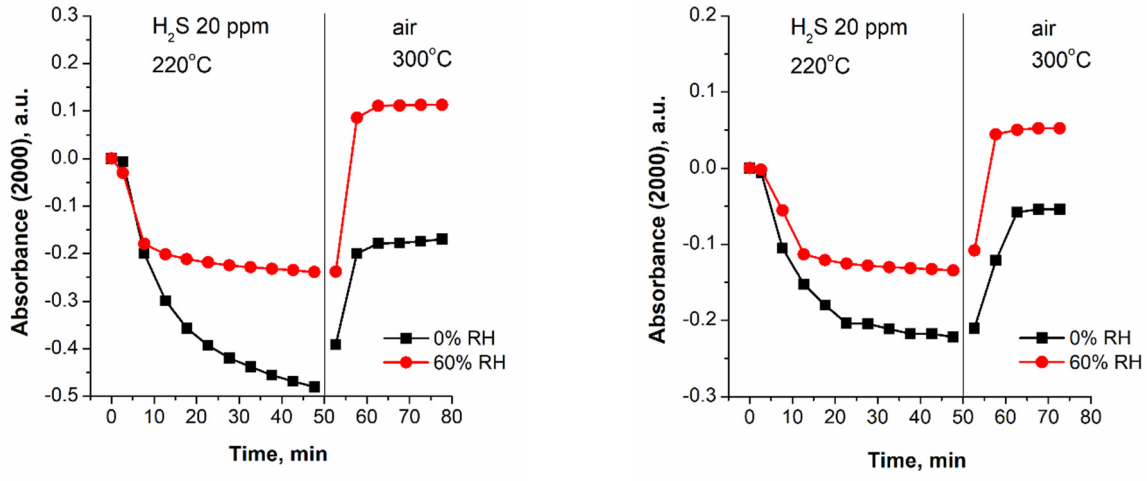

Figure 14. Baseline absorption at 2000 cm^{-1} on DRIFT spectra: (**a**) Co_3O_4; (**b**) $Ni_{0.1}Co_{2.9}O_4$.

As follows from the change in the absorption value at 2000 cm^{-1}, for both Co_3O_4 and $Ni_{0.1}Co_{2.9}O_4$ in a flow of hydrogen sulfide in dry air, the saturation electrical conductivity was lower (the resistance was higher) than in humid conditions. This means that for a long time of H_2S supply, the sensor signal should be higher in dry air. However, the conductivity curve for Co_3O_4 in humidity reaches saturation faster especially at short times (less than 10 min). The observed sensor signal (measurement for 15 min) turns out to be higher in humid air. It should be noted that the concentration of hydrogen sulfide for recording DRIFT spectra (20 ppm) is significantly higher than for sensor measurements (1 ppm) due to the different sensitivity of the methods. This should lead to an increase in the rate of all processes associated with H_2S in the DRIFT experiment.

A decrease in the sensor response time τ_{90} also indicates the processes of the sensor signal formation for Co_3O_4 in humid air are faster (Figure 15a).

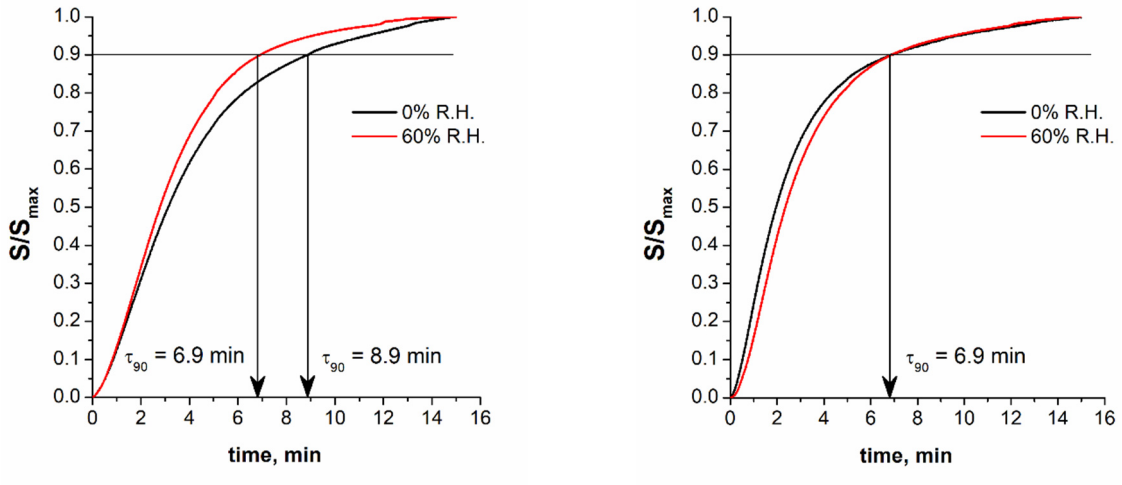

Figure 15. Sensor response time τ_{90} in dry and humid air for: (**a**) Co_3O_4; (**b**) $Ni_{0.1}Co_{2.9}O_4$.

In the case of $Ni_{0.1}Co_{2.9}O_4$, the response time to H_2S τ_{90} is the same in both dry and humid air, and coincides with that for Co_3O_4 in humidity. At the early times, the sensor signal of $Ni_{0.1}Co_{2.9}O_4$ in dry air grows even a little faster (Figure 15b). Similar trends can be seen in the DRIFT spectra (Figure 14b).

For both samples, the baseline of DRIFT spectra in dry air after the annealing cycle does not return to the initial value (Figure 14). That indicates the accumulation of sulfite and sulfate groups on the sensor surface during the detection cycles. Whereas, the sensor completely restores its original resistance in humid conditions. The observed increase in conductivity (decrease in resistance) is caused by the remove of sulfite groups during the annealing in dry air and by the increase in temperature.

4. Conclusions

In dry air, the surface of Co_3O_4 and $Ni_{0.1}Co_{2.9}O_4$ is partially covered by chemisorbed oxygen species and a relatively small number of hydroxyl groups, which can act as oxidants. Therefore, during H_2S interaction with the oxide surface, the predominant process of the oxidation is due to chemisorbed oxygen according to reaction (2), leading to the formation of SO_2 and water. This process increases the number of electrons (minority charge carriers) in the conduction band, and the resistance grows. The resulting water adsorbs on the surface and dissociates with the formation of new hydroxyl groups. On the one hand, hydroxyl groups are oxidizing agents and, on the other hand, they are more favorable as SO_2 adsorption centers than oxygen. Further oxidation of surface sulfites to sulfates by reaction (4) serves as an additional source of electrons, which increases the sensor signal at

long times. In our previous work [19], it was shown that the concentration of chemisorbed oxygen on the surface of $Ni_{0.1}Co_{2.9}O_4$ is lower than on Co_3O_4. This leads to a slowdown in the rate of reaction (2) and, as a result, led to a decrease in sensor signal toward 1 ppm H_2S with increase in Ni content.

In humid air, during dissociative adsorption of water molecules, the concentration of hydroxyl groups increases on the surface of oxides. Reactivity of the surface hydroxyl groups leads to an increase of the sensor signal with increasing of the relative humidity. The decrease in the sensor response time τ_{90} for Co_3O_4 in humid air indicates the acceleration of H_2S oxidation due to a change in the reaction mechanism, which is most likely realized with the participation of hydroxyl groups (3). The saturation state is reached when all surface hydroxyl groups are converted to hydrosulfites by reacting with SO_2. In this case, no further oxidation to sulfates was observed.

The sensor response time τ_{90} for $Ni_{0.1}Co_{2.9}O_4$ in both dry and humid air coincides in value with that for Co_3O_4 in humid air. This may indicate the participation of hydroxyl groups in the oxidation of hydrogen sulfide in both cases and the predominant of the reaction (3). In this case, an increase in the sensor signal in humidity is most likely caused by an increase in the concentration of hydroxyl groups. The signals of sulfate groups in the DRIFT spectra for $Ni_{0.1}Co_{2.9}O_4$ in dry air are less pronounced than for Co_3O_4, which also indicates that the oxidation of sulfites to sulfates occurs due to chemisorbed oxygen rather than hydroxyl groups.

Author Contributions: Conceptualization, M.R. and A.G.; methodology, M.R., K.P., A.N. and S.V.; formal analysis, K.P. and S.V.; investigation, K.P., A.N. and S.V.; data curation, K.P., A.N. and S.V.; supervision, M.R.; writing—original draft preparation, K.P. and M.R.; writing—review and editing, M.R. and A.G. All authors have read and agreed to the published version of the manuscript.

Funding: This research was funded by RFBR, grant number 18-03-00580.

Institutional Review Board Statement: Not applicable.

Informed Consent Statement: Not applicable.

Data Availability Statement: The data presented in this study are available on request from the corresponding author. The data are not publicly available due to privacy reason.

Acknowledgments: The DRIFT spectral experiments were carried out using the equipment purchased by funds of Lomonosov Moscow State University Program of the Development.

Conflicts of Interest: The authors declare no conflict of interest.

References

1. Dey, A. Semiconductor metal oxide gas sensors: A review. *Mater. Sci. Eng. B* **2018**, *229*, 206–217. [CrossRef]
2. Korotcenkov, G. Metal oxides for solid-state gas sensors: What determines our choice? *Mater. Sci. Eng. B* **2007**, *139*, 1–23. [CrossRef]
3. Llobet, E.; Brunet, J.; Pauly, A.; Ndiaye, A.; Varenne, C. Nanomaterials for the Selective Detection of Hydrogen Sulfide in Air. *Sensors* **2017**, *17*, 391. [CrossRef] [PubMed]
4. Advani, G.N.; Nanis, L. Effects of humidity on hydrogen sulfide detection by SnO_2 solid state gas sensors. *Sens. Actuators* **1981**, *2*, 201–206. [CrossRef]
5. Grossmann, K.; Pavelko, R.G.; Barsan, N.; Weimar, U. Interplay of H_2, water vapor and oxygen at the surface of SnO_2 based gas sensors—An operando investigation utilizing deuterated gases. *Sens. Actuators B Chem.* **2012**, *166*, 787–793. [CrossRef]
6. Staerz, A.; Berthold, C.; Russ, T.; Wicker, S.; Weimar, U.; Barsan, N. The oxidizing effect of humidity on WO_3 based sensors. *Sens. Actuators B Chem.* **2016**, *237*, 54–58. [CrossRef]
7. Platonov, V.; Rumyantseva, M.; Khmelevsky, N.; Gaskov, A. Electrospun ZnO/Pd Nanofibers: CO Sensing and Humidity Effect. *Sensors* **2020**, *20*, 7333. [CrossRef]
8. Wang, Y.; Duan, G.; Zhu, Y.; Zhang, H.; Xu, Z.; Dai, Z.; Cai, W. Room temperature H_2S gas sensing properties of In_2O_3 micro/nanostructured porous thin film and hydrolyzation-induced enhanced sensing mechanism. *Sens. Actuators B Chem.* **2016**, *228*, 74–84. [CrossRef]
9. Itoh, T.; Matsubara, I.; Tamaki, J.; Kanematsu, K.; Shin, W.; Izu, N.; Nishibori, M. Effect of high-humidity aging on performance of tungsten oxide-type aromatic compound sensors. *Sens. Mater.* **2012**, *24*, 13–19.

10. Shalev, G. The Electrostatically Formed Nanowire: A Novel Platform for Gas-Sensing Applications. *Sensors* **2017**, *17*, 471. [CrossRef] [PubMed]
11. Henning, A.; Molotskii, M.; Swaminathan, N.; Vaknin, Y.; Godkin, A.; Shalev, G.; Rosenwaks, Y. Electrostatic Limit of Detection of Nanowire-Based Sensors. *Small* **2015**, *11*, 4931–4937. [CrossRef]
12. Arshak, K.; Moore, E.; Lyons, G.; Harris, J.; Clifford, S. A review of gas sensors employed in electronic nose applications. *Sens. Rev.* **2004**, *24*, 181–198. [CrossRef]
13. Urasińska-Wójcik, B.; Gardner, J.W. H_2S Sensing in Dry and Humid H_2 Environment With p-Type CuO Thick-Film Gas Sensors. *IEEE Sens. J.* **2018**, *18*, 3502–3508. [CrossRef]
14. Schwarz, M.; Faisal, F.; Mohr, S.; Hohner, C.; Werner, K.; Xu, T.; Skála, T.; Tsud, N.; Prince, K.C.; Matolín, V.; et al. Structure-Dependent Dissociation of Water on Cobalt Oxide. *J. Phys. Chem. Lett.* **2018**, *9*, 2763–2769. [CrossRef] [PubMed]
15. Liotta, L.F.; Wu, H.; Pantaleo, G.; Venezia, A.M. Co_3O_4 nanocrystals and Co_3O_4–MOx binary oxides for CO, CH_4 and VOC oxidation at low temperatures: A review. *Catal. Sci. Technol.* **2013**, *3*, 3085–3102. [CrossRef]
16. Baidya, T.; Murayama, T.; Nellaiappan, S.; Katiyar, N.K.; Bera, P.; Safonova, O.; Lin, M.; Priolkar, K.R.; Kundu, S.; Rao, B.S. Ultra-low-temperature CO oxidation activity of octahedral site cobalt species in Co_3O_4 based catalysts: Unravelling the origin of the unique catalytic property. *J. Phys. Chem. C* **2019**, *123*, 19557–19571. [CrossRef]
17. Wang, H.-F.; Kavanagh, R.; Guo, Y.-L.; Guo, Y.; Lu, G.; Hua, P. Origin of extraordinarily high catalytic activity of Co_3O_4 and its morphological chemistry for CO oxidation at low temperature. *J. Catal.* **2012**, *296*, 110–119. [CrossRef]
18. Wang, Z.; Wang, W.; Zhang, L.; Jiang, D. Surface oxygen vacancies on Co_3O_4 mediated catalytic formaldehyde oxidation at room temperature. *Catal. Sci. Technol.* **2015**, *6*, 3845–3853. [CrossRef]
19. Vladimirova, S.A.; Prikhodko, K.Y.; Rumyantseva, M.N.; Konstantinova, E.A.; Chizhov, A.S.; Khmelevsky, N.O.; Gaskov, A.M. Nanocrystalline complex oxides $Ni_xCo_{3-x}O_4$: Cations distribution impact on electrical and gas sensor behavior. *J. Alloys Compd.* **2020**, *828*, 154420. [CrossRef]
20. Krotova, A.; Prikhodko, K.; Vladimirova, S.; Filatova, D. Determination of nickel, zinc and cobalt in advanced materials based on $Ni_xCo_{3-x}O_4$and $Zn_xCo_{3-x}O_4$by inductively coupled plasma mass spectrometry (ICP-MS) and X-Ray fluorescence. *Inorg. Mater.* **2019**, *55*, 1343–1346. [CrossRef]
21. Chizhov, A.; Rumyantseva, M.; Vasiliev, R.; Filatova, D.; Drozdov, K.; Krylov, I.; Marchevsky, A.; Karakulina, O.; Abakumov, A.; Gaskov, A. Visible light activation of room temperature NO_2 gas sensors based on ZnO, SnO_2 and in $2O_3$ sensitized with CdSe quantum dots. *Thin Solid Film.* **2016**, *618*, 253–262. [CrossRef]
22. World Health Organization (WHO). *Air Quality Guidelines for Europe*, 2nd ed.; WHO Regional Publications: Copenhagen, Denmark, 2000; Volume 91.
23. Davydov, A. *Molecular Spectroscopy of Oxide Catalyst Surfaces*; Wiley: Hoboken, NJ, USA, 2003; pp. 139–157.
24. Kataoka, S.; Lee, E.; Tejedor-Tejedor, M.I.; Anderson, M.A. Photocatalytic degradation of hydrogen sulfide and in situ FT-IR analysis of reaction products on surface of TiO_2. *Appl. Catal. B Environ.* **2005**, *61*, 159–163. [CrossRef]
25. Piéplu, A.; Saur, O.; Lavalley, J.-C. IR Study of H2S and SO_2 Adsorption on Ferric Oxide. *Prog. Fourier Transform. Spectrosc.* **1997**, *14*, 707–709. [CrossRef]
26. Jin, T.; Machida, M.; Yamaguchi, T.; Tanabe, K. Infrared study of sulfur-containing iron oxide. Behavior of sulfur during reduction and oxidation. *Inorg. Chem.* **1984**, *23*, 4396–4398. [CrossRef]
27. Wang, J.; Chen, L.; Ballesteros, R.L.; de la Fuente, J.M.; Domínguez, J. Evaluation of crystalline structure and SO_2 storage capacity of a series of composition-sensitive De-SO_2 catalysts. *J. Mol. Catal. A Chem.* **2003**, *194*, 181–193. [CrossRef]
28. Waqif, M.; Saad, A.M.; Bensitel, M.; Bachelier, J.; Saur, O.; Lavalley, J.-C. Comparative study of SO_2 adsorption on metal oxides. *J. Chem. Soc. Faraday Trans.* **1992**, *88*, 2931–2936. [CrossRef]
29. Laniecki, M.; Ziolek, M.; Karge, H.G. Effect of water on the formation of HSO_3—Ions upon SO_2 adsorption onto Faujasite-type zeolites. *J. Phys. Chem.* **1987**, *91*, 4–6. [CrossRef]
30. Baraton, M.-I.; Merhari, L. Determination of the gas sensing potentiality of nanosized powders by FTIR spectrometry. *Scr. Mater.* **2001**, *44*, 1643–1648. [CrossRef]
31. Du, X.; Du, Y.; George, S.M. CO Gas Sensing by Ultrathin Tin Oxide Films Grown by Atomic Layer Deposition Using Transmission FTIR Spectroscopy. *J. Phys. Chem. A* **2008**, *112*, 9211–9219. [CrossRef]